The Journal of Chemical Physics ARTICLE scitation.org/journal/jcp

Transport coefficients of the Lennard-Jones fluid close to the freezing line

Cite as: J. Chem. Phys. 151, 204502 (2019); doi: 10.1063/1.5128707
Submitted: 21 September 2019 • Accepted: 5 November 2019 •
Published Online: 25 November 2019

D. M. Heyes,[1,a] D. Dini,[1,b] L. Costigliola,[2,c] and J. C. Dyre[2,d]

AFFILIATIONS

[1] Department of Mechanical Engineering, Imperial College London, Exhibition Road, South Kensington, London SW7 2AZ, United Kingdom
[2] "Glass and Time," IMFUFA, Department of Science and Environment, Roskilde University, P.O. Box 260, DK-4000 Roskilde, Denmark

[a] **Author to whom correspondence should be addressed:** d.heyes@imperial.ac.uk
[b] **Electronic mail:** d.dini@imperial.ac.uk
[c] **Electronic addresses:** lorenzo.costigliola@gmail.com and lorenzoc@ruc.dk
[d] **Electronic mail:** dyre@ruc.dk

ABSTRACT

Molecular dynamics simulations have been carried out along four Lennard-Jones (LJ) fluid isomorphs close to the freezing line, covering a temperature, T, in the range of 0.8–350 and a number density, ρ, in the range of 1.1–3.0 in LJ units. Analysis of the transport coefficients is via the Green-Kubo time correlation function method. The radial distribution function, percolation threshold connectivity distance, self-diffusion coefficient, and shear viscosity are shown to be invariant along an isomorph to a very good approximation when scaled with Rosenfeld's macroscopic units, although there are some small departures for $T \simeq 1$ and lower temperatures. The thermal conductivity is shown for the first time also to be isomorph invariant. In contrast, the Einstein and moment-based frequencies, and especially the bulk viscosity, η_b, show poor isomorphic collapse at low T but not surprisingly tend to an "inverse power" potential limiting value in the high T limit. In the case of the bulk viscosity, the significant departures from invariance arise from oscillations in the pressure autocorrelation function at intermediate times, which scale for inverse power potential systems but not for the LJ case, at least in part, as the pressure and bulk elastic moduli are not isomorph invariant.

I. INTRODUCTION

Liquids in various applications can be subjected to extreme conditions, such as large pressure jumps, shearing, and imposed thermal gradients, sometimes simultaneously and on short time scales. As a result, the liquid structure and dynamical evolution can be perturbed significantly. To optimize performance and energy efficiency, for example, it is important to understand how these liquids respond to combinations of external perturbations. The response of the liquid is governed by a range of factors, including the equation of state and the equilibrium fluid transport coefficients (TC). This work contributes to this subject by considering the density and temperature dependence of the transport coefficients of a single component Lennard-Jones (LJ) fluid.

The transport coefficients are the self-diffusion coefficient, D, which characterizes the ease with which a single molecule translates through the liquid, the shear, η_s, and bulk, η_b, viscosities, and the thermal conductivity, λ. The last three determine the response of the liquid to imposed continuous mechanical forces and a temperature gradient, respectively. Experiments, statistical mechanical theory, and Molecular Dynamics (MD) computer simulations have been used over many decades to investigate these quantities for a range of model molecular liquids.[1] Much progress has been made in establishing the relationships between the intermolecular interactions and these properties, particularly for the popular model system based on the LJ pair potential.[1]

Levesque, Verlet, and co-workers[2,3] were the first to calculate these four transport coefficients for particles interacting with

continuous interactions, for a near triple point LJ state point using MD. Since then, many MD studies of the LJ transport coefficients have been conducted (e.g., for D,[4,5] η_s,[6,7] η_b,[8–11] and λ,[12–15]). Much of the subsequent interest has been in the self-diffusion coefficient and the shear viscosity because of their importance in understanding liquid flow behavior in general (including colloidal liquids),[1] which is important in many industrial, technical, and natural processes.

The bulk viscosity, which is also variously known as the "dilational," "compressional," or "volume" viscosity, measures the time dependent dissipative resistance of the fluid to an affine uniform change in volume. This quantity has been less well studied than the shear viscosity, in part because it is more difficult to measure experimentally. There is no direct measurement method (unlike for the shear viscosity), and it is often extracted from sound attenuation data. Although its uses are perhaps not so obvious as those of the shear viscosity, it is still an important quantity in practical applications in the fields of, for example, sound propagation and Brillouin linewidth measurements,[16] ultrasonics and shock waves,[17] and involving glass-forming liquids.[18] In many technical applications, for example, in elastohydrodynamic lubrication,[19] a liquid is subjected to a sudden pressure change whose rheological and tribological response is governed in part by the bulk viscosity.

The bulk viscosity in its own right is a fundamental physical quantity used in describing the molecular level collective dynamics of molecules in liquids, and there have been many statistical mechanical analytical treatments of it.[20–24] Analytic expressions for the wavevector dependent longitudinal viscosity ($\eta_l = \eta_b + 4\eta_s/3$) and bulk viscosity have been derived using the memory function Mori formalism.[25,26] MD simulations of the wavevector dependent bulk viscosity have also been carried out.[27] Rah and Eu derived a Stokes-Einstein-like relationship for the bulk viscosity.[28]

The search for widely applicable correlations between the bulk viscosity and other intensive liquid properties has only achieved limited success.[29] The bulk viscosity of hard spheres has been of particular interest.[30–32] Kinetic theory treatments of real molecules based on a hard sphere approximation[33] predict that the bulk viscosity should be larger than the shear viscosity at liquidlike densities. For example, the Enskog formulas for the hard sphere shear and bulk viscosities are[30]

$$\begin{aligned}\frac{\eta_s}{\eta_0} &= \frac{\rho b}{Z-1}\left(\left[1+\frac{2}{5}(Z-1)\right]^2+\frac{48}{25\pi}(Z-1)^2\right),\quad b=2\pi\sigma^3/3\\ \frac{\eta_b}{\eta_0} &= \frac{32}{15}\rho\sigma^3(Z-1),\quad \text{where}\\ \eta_0 &= 1.016\frac{5}{16\sigma^2}\left(\frac{mk_BT}{\pi}\right)^{1/2},\end{aligned}\tag{1}$$

which in the high density limit gives a value for the ratio, $\kappa = \eta_b/\eta_s$ tending to 5/3 and to zero as $\rho \to 0$. Molecular dynamics simulations, however, give a ratio of about 0.34 near the freezing transition.[34] The Enskog approach does not take account of successive correlated collisions, which are important at densities above about half the freezing density. There have been a number of MD investigations of the bulk viscosity of the Lennard-Jones fluid.[3,35–41] These have revealed that near the triple point, the bulk viscosity is also about a third of the shear viscosity,[3,11,42] whereas for liquid water, the ratio is ~2 to 3.[10,43] Therefore, at liquid densities, the ratio, κ, even for small molecule and organic liquids can range significantly on either side of unity.[29,44] The internal degrees of freedom play a much bigger role for η_b than for η_s,[10] which may in part explain this wide spread of κ.

The thermal conductivity has also been well studied for model systems by simulation[12,13] and for experimental liquids.[45] It is different to the other liquid transport coefficients in that it is finite and not small in the solid phase[46] and increases monotonically with density along an isotherm.[47,48]

There is a longstanding endeavor to collapse fluid state physical properties over a wide range of state points onto a set of master curves.[49] For example, Guggenheim[50] represented the liquid-vapor coexistence envelope of many small molecule systems as a single curve by scaling thermodynamic properties by the critical point parameters, the underlying assumption being that there is approximate conformability of small molecule intermolecular pair potentials. That work did not invoke the van der Waals equation of state. At low density, there is also a scaling of the transport coefficients based on Enskog theory.[51] More recently, an alternative scaling using the number density and temperature as proposed by Rosenfeld ("macroscopic units") has successfully revealed hidden quasiuniversality in both structural, static and dynamical properties (for example, see Refs. 49 and 52–55 and references quoted therein), which is referred to as "isomorphism," and systems that exhibit this behavior are known as "Roskilde simple" or "R-simple." An isomorph is a line of constant excess entropy for systems with strong correlations between the virial and the potential energy. Thus, the excess entropy is always an exact isomorph invariant. Only the inverse power model potential has exact invariance of structure and dynamics along isomorphs. For all other models and real fluids, the degree of invariance of the properties has to be determined by experiment or molecular modeling. For a new treatment of the entropy scaling characteristics of the transport coefficients of the LJ fluid over the whole density range, see Ref. 56. It has been found that the scaled self-diffusion coefficient and shear viscosity of the LJ fluids are to a very good approximation invariant along an isomorph for densities above approximately the critical value.[57] It is still not known whether the bulk viscosity and thermal conductivity (and some other quantities) also exhibit invariance along an isomorph. The resolution of this issue is one of the main objectives of the present study.

In Secs. II A–II D, the methodology used to compute the four transport coefficients (TC) and associated quantities is described. The Green-Kubo (GK) method is used for each TC, which requires integration of a time autocorrelation function (ACF) obtained by MD.[1] Certain property invariance along an isomorph is discussed in Sec. II E, and the MD simulation details are given in Sec. II F.

II. THEORY AND COMPUTATIONAL DETAILS

In this section, the methods used to compute the four equilibrium transport coefficients and related quantities are discussed. The simulations were carried out using the Lennard-Jones (LJ) pair potential, $\phi_{LJ}(r) = 4\epsilon[(\sigma/r)^{12} - (\sigma/r)^6]$, where ϵ and σ define the characteristic energy of interaction and diameter of the molecule,

respectively. Also the scaling behavior of the LJ potential energy and related static properties are covered. This section gives with a summary of the computational technical details.

A. Self-diffusion

The self-diffusion coefficient, D, can be calculated using the Green-Kubo (GK) formula,[1] employing the velocity autocorrelation function (VACF),

$$\begin{aligned} C_v(t) &= \langle \boldsymbol{v}(t)\cdot\boldsymbol{v}(0)\rangle, \quad D(t) = \frac{1}{3}\int_0^t \langle \boldsymbol{v}(s)\cdot\boldsymbol{v}(0)\rangle ds, \\ D &= \lim_{t\to\infty} D(t), \quad C_{n,v}(t) = \langle \boldsymbol{v}(t)\cdot\boldsymbol{v}(0)\rangle/\langle v^2\rangle, \\ D &= \frac{k_BT}{m}\tau_D, \quad \tau_D = \int_0^\infty C_{n,v}(t)\,dt, \end{aligned} \tag{2}$$

where $\boldsymbol{v}(t)$ is the velocity of an arbitrary molecule at time t, $C_v(t)$ is the VACF, k_B is Boltzmann's constant, T is the temperature, m is the mass of the particle, $C_{n,v}(t)$ is the normalized VACF, and τ_D is the relaxation or correlation time. $D(t)$ may be referred to as a time-dependent diffusion coefficient. The angular brackets indicate an average over different starting times or time origins (i.e., where $t = 0$). The trajectories of the molecules of these single trajectories build up to produce the averaged correlation function. Being a single particle property, D, has the least statistical uncertainty of the four transport coefficients for the same computational time because enhanced sampling is achieved by considering many molecules at the same time. The formally equivalent Einstein-Helfand formula[58] was also used to obtain D, but the time correlation function GK method proves to be particularly useful in the isomorphism context as the VACF is well suited to reveal small differences in the single particle dynamics along an isomorph, as will be demonstrated in Sec. III.

B. Shear viscosity

The Newtonian shear viscosity, η_s, is calculated using the GK method by[3]

$$\begin{aligned} C_s(t) &= \langle P_{xy}(0)P_{xy}(t)\rangle, \quad \eta_s(t) = \frac{V}{k_BT}\int_0^t C_s(s)ds, \\ \eta_s &= \lim_{t\to\infty}\eta_s(t), \quad \eta_s = G_\infty\tau_s, \quad C_{n,s} = C_s(t)/C_s(0), \\ \tau_s &= \int_0^\infty C_{n,s}(t)\,dt, \quad G_\infty = (V/k_BT)\langle P_{xy}^2\rangle, \end{aligned} \tag{3}$$

where $C_s(t)$ is the shear stress autocorrelation function (SACF) and $C_{n,s}(t)$ is the same function expressed in normalized form. The off-diagonal elements of the pressure tensor, e.g., P_{xy} chosen in Eq. (3), are used to determine η_s. For the monatomic LJ fluid, P_{xy} is

$$P_{xy} = \frac{1}{V}\left(\sum_{i=1}^N [m_i v_{xi}v_{yi} - \frac{1}{2}\sum_{j\neq i}^N r_{x,ij}\frac{r_{y,ij}}{r_{ij}}\phi'_{LJ}(r_{ij})]\right), \tag{4}$$

where N is the number of molecules in volume V (the volume of the simulation cell), $v_{\alpha i}$ is the α component of the velocity of molecule, i, or v_i, and $r_{\alpha,ij}$ is the α component of the pair separation vector between molecules i and j. The first derivative of the LJ pair potential, $\phi_{LJ}(r)$, is denoted by ϕ'_{LJ}. G_∞ in Eq. (3) is the "instantaneous" or infinite frequency shear rigidity modulus, and τ_s is the shear stress relaxation time.

Previous simulation calculations of $C_s(t)$ have shown that it decays monotonically to zero with time.[3,36] The so-called time-dependent shear viscosity, $\eta_s(t)$, is also defined in Eq. (3). The shear viscosity is the long time limit of $\eta_s(t)$, as defined in Eq. (3).

Equation (3) indicates that η_s can be written as the product of a modulus, G_∞, times a relaxation time, τ_s, a decomposition that dates back to Maxwell and his work on gas viscosity.[59] Zwanzig and Mountain (ZM)[60] derived for the LJ potential an explicit alternative formula for G_∞ in terms of the time-averaged pressure and energy of the system,

$$\begin{aligned} G_\infty &= \frac{26}{5}\rho k_BT + 3P - \frac{24}{5}\rho e \\ &= 3P - \frac{24}{5}\rho u - 2\rho k_BT, \end{aligned} \tag{5}$$

where u is the average potential energy per particle, $e = u + 3k_BT/2$, and $\rho = N/V$ is the number density. The first formula above is taken from the Zwanzig and Mountain (ZM) article, while the second is from Ref. 3. Alternative equivalent formulas for G_∞ of the LJ fluid in terms of the average potential energy per particle from the repulsive and attractive parts of the potential have also been derived,[36,61] which are more useful in the present context,

$$\begin{aligned} G_\infty &= \rho k_BT + \frac{\rho}{15}(108u_{12} - 18u_6), \\ u_{12} &= \frac{1}{2N}\left\langle \sum_{i=1}^N \sum_{1,j\neq i}^N 4r_{ij}^{-12}\right\rangle, \\ u_6 &= \frac{1}{2N}\left\langle \sum_{i=1}^N \sum_{1,j\neq i}^N 4r_{ij}^{-6}\right\rangle, \end{aligned} \tag{6}$$

where u_{12} (repulsive part) and u_6 (attractive part), which can be obtained directly from the simulation or indirectly from the interaction or configurational parts of the pressure (P_c) and total energy (u),

$$\begin{aligned} u_{12} &= \frac{P_c - 2\rho u}{2\rho}, \\ u_6 &= \frac{P_c - 4\rho u}{2\rho}, \end{aligned} \tag{7}$$

where $u = u_{12} - u_6$ (note that u_6 is defined as a positive quantity). Equation (7) follows directly from the definition of u and the virial expression for the pressure, $P = \rho k_BT + P_c$.[1] The definition of G_∞ in Eq. (6) is more useful in the context of isomorphic scaling as u_{12} and u_6 play a pivotal role (see, e.g., Ref. 62 in which the repulsive and attractive potential energy terms are plotted for the Kob-Andersen LJ system). This is discussed further in Sec. II E.

C. Bulk viscosity

The bulk viscosity is defined through the macroscopic relation, $\Delta = -\eta_b\nabla\cdot\boldsymbol{u} = -\eta_b[\dot{V}/V]$, in the $\dot{V}/V \to 0$ limit. In the equation, $\Delta = \mathrm{Tr}\,P - \mathrm{p}$, with P, the pressure tensor, p, the hydrostatic pressure, $\boldsymbol{u}$ is the fluid velocity, V is the volume, and $\dot{V}$ is the time derivative

of the volume.[28,41] The bulk viscosity was calculated using a Green-Kubo formula involving the deviatoric pressure, as follows.[9,24,63,64] The pressure, P, is

$$P = \frac{1}{3V}\left(\sum_{i=1}^{N}[m_i v_i^2 - \frac{1}{2}\sum_{j\neq i}^{N} r_{ij}\phi'_{LJ}(r_{ij})]\right), \tag{8}$$

and the deviatoric pressure in a constant N ensemble is[64]

$$\delta P(t) = P(t) - \overline{P} - \frac{1}{V}\left\{\left(\frac{\partial \overline{P}}{\partial e}\right)_{\rho}[E(t) - \overline{E}]\right\}, \tag{9}$$

where e is the internal energy per unit volume.[42] The time average value of the total energy and pressure is $\overline{E}$ and $\overline{P}$, respectively. The final term in the definition of the deviatoric pressure, $\delta P(t)$, is zero in the NVE or constant total energy, E ensemble, as then $E(t) = \overline{E}$. With the Verlet leapfrog time integrator, E, does fluctuate with time to a small extent even in a nominally NVE simulation. It is the so-called *shadow energy* that is constant.[65,66] Nevertheless, the standard deviation of the fluctuations of $E(t)$ is relatively small compared with that of its components, the potential energy and kinetic energy. Therefore, the relatively small fluctuations in E with time in an NVE MD simulation have an insignificant effect on the (small) value of the last term in Eq. (9).

For the bulk viscosity, we have[9,24,40,41,64]

$$\begin{aligned} C_b(t) &= \langle \delta P(0)\delta P(t)\rangle, \quad \eta_b = \frac{V}{k_B T}\int_0^{\infty} C_b(t)dt, \\ \eta_b &= (K_\infty - K_0)\tau_b, \quad C_{n,b} = C_b(t)/C_b(0), \\ \tau_b &= \int_0^{\infty} C_{n,b}(t)\, dt, \quad K_\infty - K_0 = (V/k_B T)\langle \delta P^2\rangle, \end{aligned} \tag{10}$$

where $C_b(t)$ is the deviatoric pressure autocorrelation function, BACF (where the B stands for bulk viscosity). Also, K_∞ and K_0 are the infinite frequency adiabatic bulk modulus and zero frequency adiabatic bulk modulus, respectively.

D. Thermal conductivity

The thermal conductivity, λ, is obtained from the GK relationship involving the heat flux vector, J_q,[67]

$$\boldsymbol{J}_q = \frac{1}{V}\left(\sum_{i=1}^{N}[e_i \boldsymbol{v}_i - \frac{1}{2}\sum_{j\neq i}^{N}(\boldsymbol{r}_{ij}\cdot\boldsymbol{v}_{ij})\frac{\boldsymbol{r}_{ij}}{r_{ij}}\phi'_{LJ}(r_{ij})]\right), \tag{11}$$

where

$$e_i = \frac{1}{2}m_i v_i^2 + \frac{1}{2}\sum_{j\neq i}\phi(r_{ij}) \tag{12}$$

is the energy of a molecule in the fluid, and $v_{ij} = v_i - v_j$ is the relative velocity between molecules i and j. The thermal conductivity and related quantities are[67,68]

$$\begin{aligned} C_\lambda(t) &= \frac{1}{3}\langle \boldsymbol{J}_q(0)\cdot\boldsymbol{J}_q(t)\rangle, \quad \lambda = \frac{V}{k_B T^2}\int_0^{\infty} C_\lambda(t)dt, \\ \lambda &= M_\infty^T \tau_\lambda, \quad C_{n,\lambda} = C_\lambda(t)/C_\lambda(0), \\ \tau_\lambda &= \int_0^{\infty} C_{n,\lambda}(t)\, dt, \quad M_\infty^T = \frac{V}{3k_B T^2}\langle \boldsymbol{J}_q^2\rangle, \end{aligned} \tag{13}$$

where $C_\lambda(t)$ is the heat flux autocorrelation function, TACF, and M_∞^T, which is referred to as the thermal "modulus" to be consistent in terminology with the corresponding shear and bulk viscosity ($t = 0$) quantities.

The moduli for the bulk viscosity and the thermal conductivity are most conveniently obtained from the fluctuation formulas given in Eqs. (10) and (13), respectively. There is not a Zwanzig-Mountain formula corresponding to Eq. (5) for G_∞, as the η_b and λ "moduli" involve a component of the equilibrium equation of state (i.e., a zero-frequency property).

E. Static quantities including the moduli

Consider the generalized LJ potential, $\phi(r) = 4\epsilon[(\sigma/r)^{2n} - (\sigma/r)^n]$, where the coefficient in the potential definition is 4 so that the minimum potential energy is $-\epsilon$. Using the formula for the average potential energy in terms of the radial distribution function,

$$\begin{aligned} u &= 2\pi\rho\int_0^{\infty}\phi(r)g(r)r^2\, dr, \\ &= 8\pi\epsilon\int_0^{\infty}\left(\frac{\rho^{2n/3}}{\tilde{r}^{2n}} - \frac{\rho^{n/3}}{\tilde{r}^n}\right)g(\tilde{r})\tilde{r}^2\, d\tilde{r}, \\ &= A\epsilon\rho^{2n/3} - B\epsilon\rho^{n/3} = u_{2n} - u_n, \\ \text{where} \quad A &= 8\pi\int_0^{\infty} g(\tilde{r})\tilde{r}^{2-2n}\, d\tilde{r}, \quad B = 8\pi\int_0^{\infty} g(\tilde{r})\tilde{r}^{2-n}\, d\tilde{r}, \end{aligned} \tag{14}$$

where $\tilde{r} = r\rho^{1/3}$. The parameters, A and B, are constant along an isomorph as $g(\tilde{r})$ is invariant along that line. Rosenfeld was the first to propose and exploit in a number of papers that thermodynamic properties and liquid-solid coexistence[69,70] and transport properties[71] could be expressed as a linear combination of inverse power potential (IP) terms, which is embodied in Eq. (14). It is notable that $\tilde{u} = u/k_B T$ is not invariant along an isomorph as the two density-dependent terms in Eq. (14) have different exponents and consequently the relative contribution to $\tilde{u}$ from the repulsive and attractive parts of the potential varies with density (temperature) along the isomorph. The stages in Eq. (14) parallel those given in Schrøder *et al.*[72] Although $\tilde{u}$ is not an isomorph invariant (as was also discussed in Ref. 73), the constants A and B in Eq. (14) are invariant along an isomorph, a situation that may be referred to as the *implicit invariance* of u.

As for the total potential energy, for the $2n$:n potential, the pressure and infinite frequency (or "instantaneous") elastic moduli[61] can also be expressed in terms of ρ, T, u_{2n}, and u_n. Following Eqs. (6) and (14), we have

$$\begin{aligned} \tilde{u} &= \frac{u}{k_B T} = A\frac{\rho^{2n/3}}{T} - B\frac{\rho^{n/3}}{T}, \\ \tilde{P} &= \frac{P}{\rho k_B T} = 1 + 2nA\frac{\rho^{2n/3}}{T} - nB\frac{\rho^{n/3}}{T}, \\ \tilde{G}_\infty &= \frac{G_\infty}{\rho k_B T} = 1 + \frac{2n(2n-3)}{15}A\frac{\rho^{2n/3}}{T} - \frac{n(n-3)}{15}B\frac{\rho^{n/3}}{T}, \\ \tilde{K}_\infty &= \frac{K_\infty}{\rho k_B T} = \frac{5}{3} + \frac{2n(2n+3)}{9}A\frac{\rho^{2n/3}}{T} - \frac{n(2+3)}{9}B\frac{\rho^{n/3}}{T}, \end{aligned} \tag{15}$$

for a number of static quantities and where $k_B T$ is replaced by ϵT (the usual definition of temperature in LJ units). The $\tilde{u}$, $\tilde{P}$ quantities, $\tilde{G}_\infty$, and $\tilde{K}_\infty$ are *not* invariant along an isomorph. These quantities for the inverse power potential case [i.e., where the $n-$ term is

omitted from Eq. (15)] are, in contrast, invariant along an isomorph. Note that $n > 3$ is a restriction for thermodynamic stability.[74]

The invariance of $g(\tilde{r})$ along an isomorph leads directly to other properties that depend on the radial distribution functions (RDF) (according to the standard statistical mechanical formulas) also being invariant or implicitly invariant, e.g., the two body contribution to the excess entropy.[75]

F. Simulation details

The output quantities of the MD calculations were in the usual LJ units of ϵ, σ, and the unit of mass is the mass of each molecule, m. A constant time step in macroscopic[76–78] or isomorph units (IU) was used, where the LJ units time step is $\Delta t = \Delta t_0\, T^{-1/2}\rho^{-1/3}$, which takes account of isomorphic scaling of time and therefore ensures that the same exploration of phase space in these reduced units is carried out along the isomorph. The reference time step at state point $\tilde{\rho} = 1$ and $\tilde{T} = 1$ was $\Delta t_0 = 0.0015$. The interaction truncation distance, r_c, was 3.2,[79] in some simulations, and $r_c = r_0(\rho_0/\rho)^{1/3}$, where $\rho_0 = 2.5$ and ρ_0 is the lowest density in the sequence, in most of the simulations.

The number of particles in the simulation cell, N, was for most cases, 864, and $N = 2048$ and 4000 particles were used in some simulations to assess the system size dependence of the results. The initial configuration for the lowest density in each isomorph series was assembled by random particle insertion to form an amorphous starting structure in the simulation box. The computations were conducted for typically 100×10^6 time steps for $N = 864$ and 10×10^6 time steps for $N = 2048$ and $N = 4000$ for each state point during the postequilibration stage. Simulations were carried out using both NVE and NVT dynamics, where in the latter case the Nosé-Hoover thermostat was employed,[80] with a time constant of 3 LJ time units. Statistical uncertainties in the means were determined using block averaging.[81]

The isomorph densities and temperatures were determined using the analytical formula

$$T(\rho)/T_0 = (\gamma_0/2 - 1)(\rho/\rho_0)^4 - (\gamma_0/2 - 2)(\rho/\rho_0)^2, \qquad (16)$$

which gives the isomorph through the state point (ρ_0, T_0) at which the density-scaling exponent, γ_0, at this reference state point is calculated from the standard fluctuation expression [e.g., see Eq. (1) in Ref. 82 and the definition in Eq. (19)]. Equation (16) traces out a configurational adiabat (i.e., a curve of constant excess entropy, S^{ex}) from the reference starting point on the phase diagram of the LJ system. Note that not all configurational adiabats are isomorphs, only the ones where the virial-potential-energy Pearson coefficient, R, is close to 1. In the following discussion, quantities will be referred to as being "unscaled" when given in LJ units and "scaled" when in macroscopic or IU "reduced" units.

III. RESULTS AND DISCUSSION

In this section, the scaling properties of the four transport coefficients and other (sometimes related) quantities along four isomorphs are explored. The factors required to convert the various quantities from LJ to isomorph reduced units (IU) are given in Table I. For a quantity X in LJ units, the IU scaled quantity is denoted by $\tilde{X}$. Figure 1 indicates the ρ, T state points used in the simulations and marks out the surrounding phase boundaries. The four isomorphs were in the fluid phase and labeled I1 to I4. The temperature and densities for the I1 state points are given in Table II, and the corresponding values for I2 to I4 are given in supplementary material. The isomorphs are almost parallel to the freezing line (as shown in Refs. 83 and 84). A full theory for the melting line of the LJ system was derived in Ref. 85. For ease of plotting, the liquid-vapor and fluid-solid coexistence lines obtained from many simulation studies were fitted to the following semiempirical formulas. Denoting l for liquid and v for vapor, the liquid-vapor boundary line shown in Fig. 1 was produced using the formula

$$\begin{aligned}
\rho_l(T) &= \rho_c + a_l(T_c - T)^{1/3} + b_l(T_c - T) + c_l(T_c - T)^{3/2},\\
\rho_v(T) &= \rho_c + a_v(T_c - T)^{1/3} + b_v(T_c - T) + c_v(T_c - T)^{3/2},\\
\text{where}\quad & a_l = 0.347\,590,\ \ b_l = 0.647\,553,\ \ c_l = -0.355\,848,\\
& a_v = -0.380\,826,\ \ b_v = -0.310\,175,\ \ c_v = 0.412\,449,
\end{aligned} \qquad (17)$$

TABLE I. Units and conversion factors. To convert a quantity in LJ units into isomorph units, multiply the quantity in LJ units (the second column) by the term in the third column ($k_B = 1$).

Quantities	LJ units	Isomorph scaling factor
r	σ	$\rho^{1/3}$
t	$\sigma(m/\epsilon)^{1/2}$	$\rho^{1/3}T^{1/2}$
D	$\sigma(\epsilon/m)^{1/2}$	$\rho^{1/3}T^{-1/2}$
η_s, η_b	$\sigma^{-2}(\epsilon m)^{1/2}$	$\rho^{-2/3}T^{-1/2}$
u	ϵ	T^{-1}
P, G_∞, $(K_\infty - K_0)$	$\epsilon\sigma^{-3}$	$\rho^{-1}T^{-1}$
λ	$\sigma^{-2}(\epsilon/m)^{1/2}$	$\rho^{-2/3}T^{-1/2}$

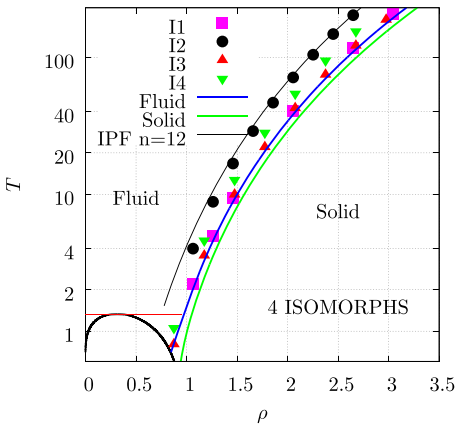

FIG. 1. Positions of the isomorphic state points used in this study on the ρ, T Lennard-Jones phase diagram. The phase boundary coexistence lines were generated from the approximate expressions given in Eqs. (17) and (18) for the liquid-vapor and fluid-solid, respectively. State points along the four isomorphs, I1, I2, I3, and I4 are shown. The figure also shows the isomorph of the IPF ($n = 12$) fluid as a thin black curve, produced from the formula, $T(\rho) = T_0(\rho/\rho_0)^4$, for the I2 isomorph densities using its highest point values for the reference state, i.e., $\rho_0 = 3.045\,44$ and $T_0 = 358.64$.

TABLE II. Key static properties of the $N = 864$ simulated systems along the I1 isomorph are given. Where no errors are given, they occur in the not shown next digit. The simulations were carried out in the *NVT* ensemble. Note that the $\tilde{u}$ and $\tilde{P}$ are not isomorph invariant.

T	ρ	u_{12}	$-u_6$	u	P	$\tilde{u}$	$\tilde{P}$
2.2000	1.0635	13.97	−18.56	−4.5959(1)	22.27	−2.089	9.518
4.9179	1.2617	27.61	−26.08	1.5278(2)	79.71	0.311	12.846
9.4388	1.4599	49.46	−34.89	14.564(4)	200.7	1.543	14.564
40.593	2.0545	193.9	−69.03	124.86	1 393	3.076	16.703
116.22	2.6491	536.0	−114.7	421.24	5 379	3.625	17.471
205.58	3.0455	936.3	−151.6	784.62(1)	11 107	3.817	17.742

which is a reparametrization of the formula of Lofti *et al.*[86] The new constants in Eq. (17) were determined by least squares fitting to more recent simulation derived coexistence data which were not available at the time to Lofti *et al.* (see the source references given in Ref. 87, which typically took the largest cutoff in each study, usually greater than 3.5). The critical point parameters used in the fitting process are $T_c = 1.326(2)$ and $\rho_c = 0.316(2)$.[88]

The freezing (f) or liquidus and melting or solidus (s) lines in Fig. 1 were obtained by least squares fitting of coexistence simulation data referenced in Ref. 89 and more recent coexistence points[90,91] to the formulas

$$
\begin{aligned}
&T'_f(\rho) = A_f\rho^4 + B_f\rho^2,\\
&T'_s(\rho) = A_s\rho^4 + B_s\rho^2,\\
&T_f(\rho) = \left(1.0 - C_f \exp(-D_f T'_f(\rho))\right) T'_f(\rho),\\
&T_s(\rho) = \left(1.0 - C_s \exp(-D_s T'_s(\rho))\right) T'_s(\rho),\\
&A_f = 2.350\,884,\ B_f = -0.878\,513,\ C_f = -1.027\,577,\ D_f = 2.694\,397,\\
&A_s = 2.084\,485,\ B_s = -1.108\,135,\ C_s = 7.927\,262,\ D_s = 6.652\,411.
\end{aligned}
\tag{18}
$$

See Refs. 83, 85, and 92–94 for the formulas on the first two lines of Eq. (18), which are supplemented by the formulas on the third and fourth lines of Eq. (18) to enable analytic matching the simulation data for T less than about 1.0. For higher temperatures, the supplemented formulas are hardly distinguishable in the first two lines. Reference 85 derives more formally exact expressions for the two coexistence lines.

Figure 1 also shows an isomorph of the inverse power fluid (IPF), where $n = 12$, and starting from the I2 isomorph at its highest point density and temperature used as the reference state (see the figure caption for further details). The IPF isomorph line gradually goes above the I2 state points with decreasing density. The progressive deviation between the LJ and IPF system isomorphs reflects the fact that the LJ potential has a higher effective IPF exponent toward the triple point (approaching 18[95]).

Figure 2 shows the Pearson coefficients relevant to isomorphism as a function of density along the four isomorphs,

$$\gamma(\rho, T) = \frac{\langle \Delta W \Delta U \rangle}{\langle (\Delta U)^2 \rangle}, \tag{19}$$

where $\Delta X = X - \langle X \rangle$, $W = PV - Nk_BT$, and γ is referred to as the density-scaling exponent. The other relevant Pearson coefficient is

$$R(\rho, T) = \frac{\langle \Delta W \Delta U \rangle}{\sqrt{\langle (\Delta W)^2 \rangle \langle (\Delta U)^2 \rangle}}. \tag{20}$$

Figure 2 reveals that γ decreases slowly with increasing density toward a limit of 4 and $R \simeq 1$ to a very good approximation along the whole isomorph in each case (apart perhaps from small deviations for $T < 1$). At high temperature, the isomorph tends to that of an inverse power potential (IP) ($\sim r^{-n}$) fluid with the exponent, $n = 3\gamma$ (i.e., 12 here) and $R = 1$. For other fluids, the criterion, $R > 0.9$, has been used as a practical definition of R-simple fluids.[96] At high density and temperature, the Lennard-Jones system approaches the inverse power 12 potential in its properties, but the isomorph of non-IP systems extends to much lower densities and temperature than might be expected, because the effective ("IP") exponent 3γ varies along the isomorph (increasing with decreasing density). Hence, the successful observation of isomorphic invariance in non-inverse power fluids is because the ρ, T line takes a different path on the phase diagram than that of an IP system with an exponent (in the LJ case) equal to 12.

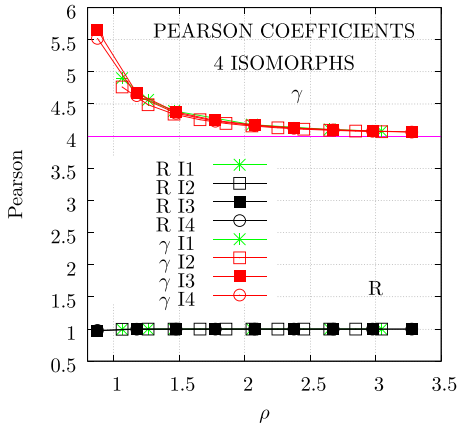

FIG. 2. The Pearson coefficients, γ, defined in Eq. (19), and R, defined in Eq. (20), as a function of density along the 4 isomorphs.

A. Structural properties and the percolation threshold

Two probes of the local structure are used to test for invariance along the isomorphs. Radial distribution functions (RDFs) are shown in Fig. 3(a) for three state points of the I1 isomorph sequence, the lowest and highest density cases and one in the middle (see Table II). Both distance unscaled and IU scaled RDFs are given in the figure. The three RDFs scale very well at most distances, although there are small differences between the three at the apex of the first peak, which shows up more clearly in the lowest set of curves in the figure that show $g(T,\tilde{r}) - g(T = 206,\tilde{r})$, i.e., the difference in the RDF at a given temperature from its value for the highest temperature example. The invariance of structure is a subtle effect

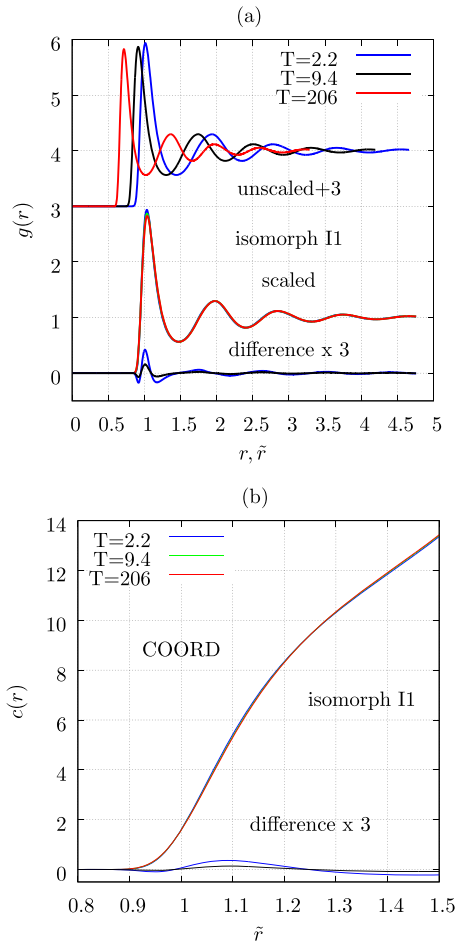

FIG. 3. Frame (a), the distance IU scaled radial distribution function for three of the I1 isomorph state points. Key: Distance unscaled data at the top (shifted upward by 3) and IU distance scaled data in the middle. At the bottom is shown the difference in the scaled RDF, $g(\tilde{r})$, for T = 2.2 minus that from T = 206 (blue), and T = 9.4 minus that from T = 206 (black). The differences are multiplied by 3 in the figure to clarify the small differences. The MD simulations were for N = 864 particles. (b) as for frame (a), except that the accumulated radial coordination number, $c(r)$, is shown as a function of the IU scaled distance. As for the RDF, the differences are multiplied by 3 for clarity.

that results from the invariance of the total force on any given particle (in IU reduced units) due to nonobvious cancellations of contributions from the many (10–14) nearest neighbors.[73,97] For very short distances, however, the probability is dominated by the Boltzmann factor of the single particle pair in question. This factor is not isomorph invariant. Consequently, the details of the decay of $g(r)$ to zero at very short distances are not expected to be isomorph invariant, in fact the decay is sharper, the larger γ is. Now, if the total number of particles within the first coordination shell is isomorph invariant, some of the "missing" part from $g(r)$ at short distances (for large γ) must have moved elsewhere so the peak value of $g(r)$ increases slightly along an isomorph on moving in the direction of increasing γ (typically toward lower densities). The particles shift slightly to larger separations as the density decreases, which is what is observed in Fig. 3(a), and has been seen for many other systems (e.g., see Fig. 9(d) in Ref. 83). Figure 3(b) presents the accumulated coordination number, $c_n(r) = 4\pi\rho\int_0^r x^2 g(x)dx$, which has not been plotted before in the context of isomorphism, as far as we are aware. It is basically a monotonically increasing function with r and exhibits excellent invariance when distance is scaled with the macroscopic unit, as might be expected from the similar behavior in $g(r)$. The integral, $c_n(r)$, forms the basis of the Kirkwood-Buff integrals widely used in the theory of mixtures of two or more types of molecule,[98] which could potentially be used to formulate isomorphic scaling criteria of mixtures, such as the binary LJ Kob-Andersen example.[99]

Another quite different probe of the local structure derives from partitioning the particles into clusters, using the Stillinger criterion for deciding whether a particle is or is not in a cluster.[100] This procedure declares that any particle that is less than a certain distance, σ', from any particle already in the cluster, is also in the cluster. The value of σ' when half the configurations generated in the simulation give rise to at least one cluster which spans the whole periodic system is taken to be the percolation connectivity distance, σ_p. This characteristic distance has been computed a number of times for various model molecular systems with different pair potentials as a function of thermodynamic state point (see Ref. 101 and citations therein).

Figure 4 compares the unscaled and IU scaled value of σ_p for the six state points along the isomorph I1. The scaled data, at the top of the figure, are seen to take the form of a horizontal line, and the unscaled data monotonically decays with increasing density (shown in the lower part of the figure). Therefore, the percolation threshold connectivity distance, σ_p, is also isomorph invariant to a very good approximation. As this quantity is a reflection of the relative positions of the particles on both short and long length scales, the IU scaling of σ_p suggests that all higher order m–body positional distribution functions[1] should also scale using the IU factors. This is consistent with the invariance of the Boltzmann canonical probabilities along an isomorph that constituted the original 2009 isomorph definition,[102] which is now in the improved theory of 2014,[103] a consequence of defining an isomorph to be a line of constant excess entropy.

A consequence of the invariant structure along an isomorph as revealed in Eq. (14) is that $A = u_{12}/\rho^4$ and $B = u_6/\rho^2$ should be constant along an isomorph. Figure 5 presents $A(\rho)$ in frame (a) and $B(\rho)$ in frame (b), which shows that invariance is found, apart from where $T < 1$, for u_{12} and slightly less so for u_6. This is consistent with

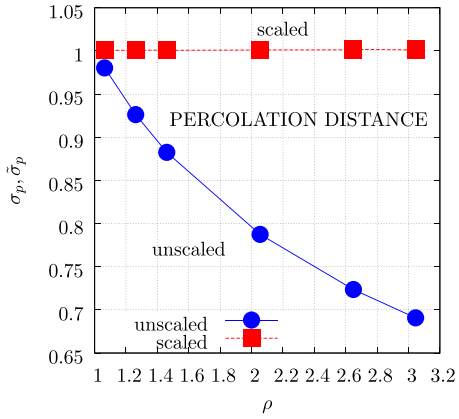

FIG. 4. The percolation connectivity distance, σ_p, for the I1 isomorph state points in both unscaled and IU scaled distance units. The MD simulations were for $N = 864$ particles.

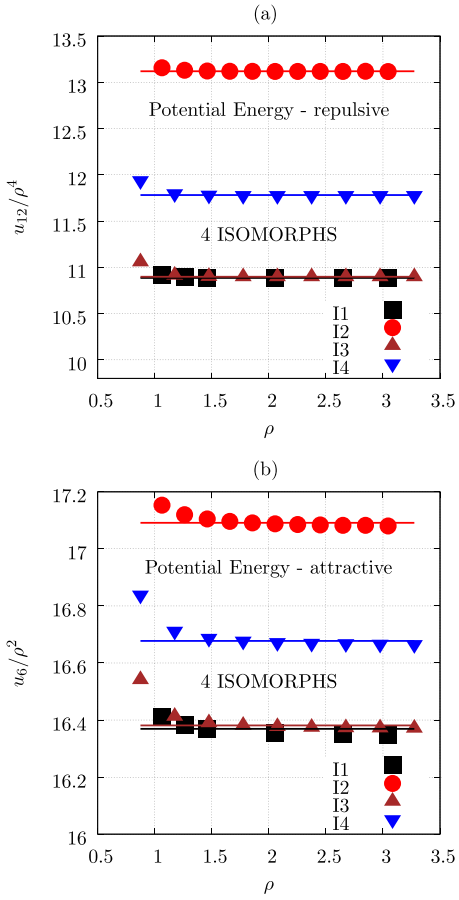

FIG. 5. Frame (a) is the density dependence of the parameter, $A = u_{12}/\rho^4$, from Eq. (14) for the four isomorphs. The A values represented by the horizontal lines have A values of 10.9, 13.1, 10.9, and 11.8 for I1 to I4, respectively. In frame (b) is shown $B = u_6/\rho^2$ for $N = 864$ for the four isomorphs. The average B values are 16.4, 17.1, 16.4, and 16.7, respectively. The LJ fluid was used and $N = 864$. Equation (6) gives the definitions of u_{12} and u_6.

there being a shift of the particles to short distance as revealed in the $g(r)$ in Fig. 3, as temperature decreases and reflects that $g(r)$ has small deviations from isomorphic scaling for $r \simeq 1.0$. Table II gives u, $\tilde{u}$, P, and $\tilde{P}$ for the I1 isomorph, which confirms that the energy and pressure themselves are not isomorph invariant (as proved formally in Sec. II E).

B. Normalized time correlation functions and relaxation times

This section investigates the isomorphic scaling behavior of the normalized time correlation functions used in the GK formulas for the four transport coefficients. Figure 6(a) presents the normalized VACF of three of the state points along the isomorph

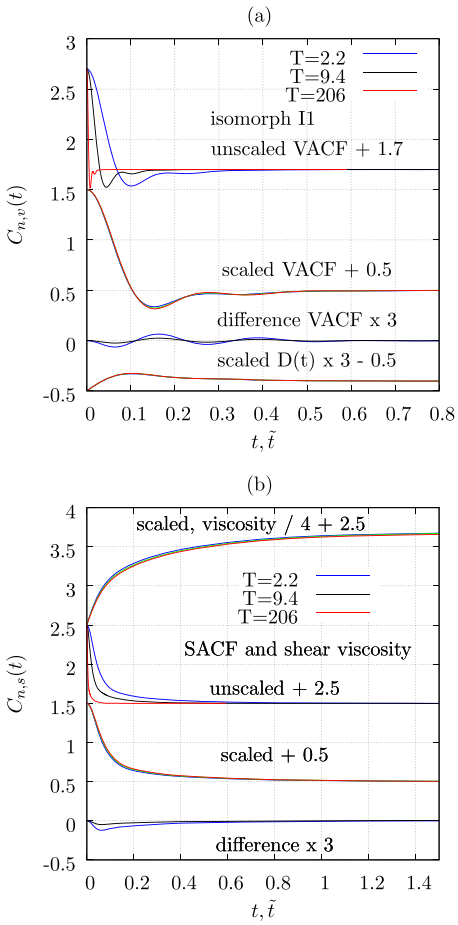

FIG. 6. Frame (a) is the normalized diffusion coefficient VACF defined in Eq. (2) in both LJ time and IU scaled units for isomorph I1. The second set of curves from the bottom is $C_{n,v}(\tilde{t})$ for $T = 2.2$ minus that from $T = 206$ (blue) and $T = 9.4$ minus that from $T = 206$ (black). The differences are multiplied by 3 to make them more visible. The bottom set of curves (which are hardly distinguishable) are the $\tilde{D}(\tilde{t})$. In frame (b), the I1 isomorph normalized shear viscosity SACF defined in Eq. (3) and related data are plotted. The time-dependent viscosity, $\tilde{\eta}_s(\tilde{t})$, is plotted in the top set of curves.

I1 in unscaled and IU scaled units. Just as for the three RDFs from the state points in Fig. 3, the corresponding three VACFs collapse very well in IU reduced time. There are, however, some small differences [just like for $g(r)$] that are not statistical in origin. These show up in the second set of curves from the bottom, which indicates that $C_v(T,\tilde{t}) - C_v(T = 206,\tilde{t})$ are oscillatory for the two lower temperatures (note that these differences are scaled by a factor of 3 in the figure to highlight the differences). However, these small departures from scaling do not have any noticeable effect on the time dependent diffusion coefficient, $D(t)$ [the lowest set of curves in Fig. 6(a)], presumably because of the cancellation of the differences in the VACF when integrated across the time domain. At short times, in the "ballistic" region, the VACF and mean-square displacement exhibit macroscopic unit scaling by definition of the unit system.[104] This may help explain why the back-scattering or caging effect seen in the VACF still gives rise to macroscopic unit scaling of the time dependent diffusion coefficient.

Figure 6(b) gives the same decomposition for the normalized shear viscosity SACF. In this case, the "difference" curves are systematic along the isomorph, and not oscillatory, which leads to a more prominent (but still relatively small) difference between the three time-dependent viscosities [shown in the top set of curves of Fig. 6(b)].

Figure 7(a) presents the thermal conductivity TACF of three of the state points along the isomorph I1, in unscaled and scaled units. Just as for the SACF, there is a small nonoscillatory systematic difference between the TACF in IU scaled time for the state points (they decay more rapidly with decreasing temperature), but this has a relatively small effect on the thermal conductivity obtained by the integration of the TACF in Eq. (13).

Figures 6(a), 6(b), and 7(a) demonstrate that the normalized ACF of molecule velocity, shear stress, and heat flux collapse well onto the same curve when expressed in terms of IU time units, provided the temperature is not too low (i.e., not below ~≃1.0), and even then the differences are relatively minor. Comparison with Fig. 2 confirms that the less invariant part of the phase diagram is in the low temperature limit where R is less than unity.

Figure 7(b) shows the deviatoric pressure autocorrelation function, BACF, in IU reduced time in the NVE ensemble for the six I1 isomorph state points. Hoheisel showed by MD that the LJ BACF for high density fluids takes on an oscillatory form,[105] and this is what we see here. The figure shows $C_{n,b}(\tilde{t}) < 0.08$ with time on a log scale. In this case, the collapse of the normalized BACF is not good at intermediate times near where the minima and maxima appear. The depth of the minima increases with temperature and is therefore not invariant along the isomorph. The initial decay and limiting long time BACF regions (for reduced times greater than ~0.4) do exhibit very good invariance, however. It is also noteworthy that the time of the first minimum and subsequent minima in IU is the same for the six state points (although the $T = 2.2$ maximum is a little shifted inward compared with the rest). Therefore, there are some aspects of the LJ BACF that are isomorph invariant.

To help elucidate this issue, for comparison, simulations were carried out with an IPF ($n = 12$) potential. This system exhibits bulk viscosity invariance, as it should [see Fig. 8(a) and details in the caption] as do the other transport coefficients. Figure 8(b) shows the BACF for the IP system in scaled time units. Significantly, the BACF

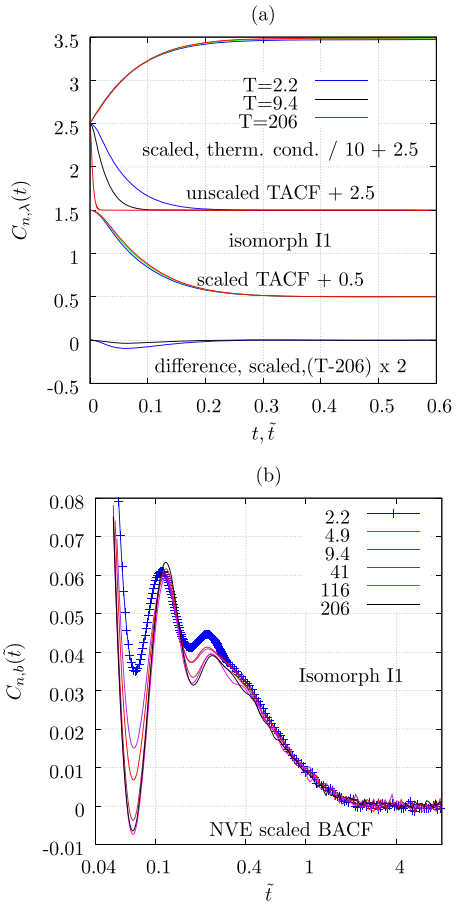

FIG. 7. Frame (a) is as for Fig. 6(b), except the TACF and thermal conductivity data are plotted, the quantities being defined in Eq. (13). The time-dependent reduced thermal conductivity, $\tilde{\lambda}(\tilde{t})$, is plotted in the top set of curves. Frame (b) shows the normalized BACF defined in Eq. (10) for the six state points of isomorph I1 carried out using NVE MD dynamics. The scale is log-lin, and only the $C_{n,b}(\tilde{t}) < 0.08$ data are shown to highlight the oscillatory region of the BACF which does not IU scale. The temperatures are given in the figure.

are also highly oscillatory at intermediate times, but these nevertheless show isomorphic invariance. Therefore, it is not that there are oscillations in the BACF which is responsible for the invariance but that they are not invariant for the LJ fluid but are for the IP fluid. The shear viscosity and thermal conductivity ACF decrease monotonically with time, and it is only the BACF of the collective property time correlation functions that decays in a damped oscillatory fashion. An analysis of the consequences of these trends for the corresponding transport coefficients is made in Sec. III D. First, we consider in Sec. III C two measures of the short time behavior of the ACFs.

C. Short time characteristics of the time correlation functions

There are two widely used measures of the short time scale relaxation behavior, which can be expressed as characteristic

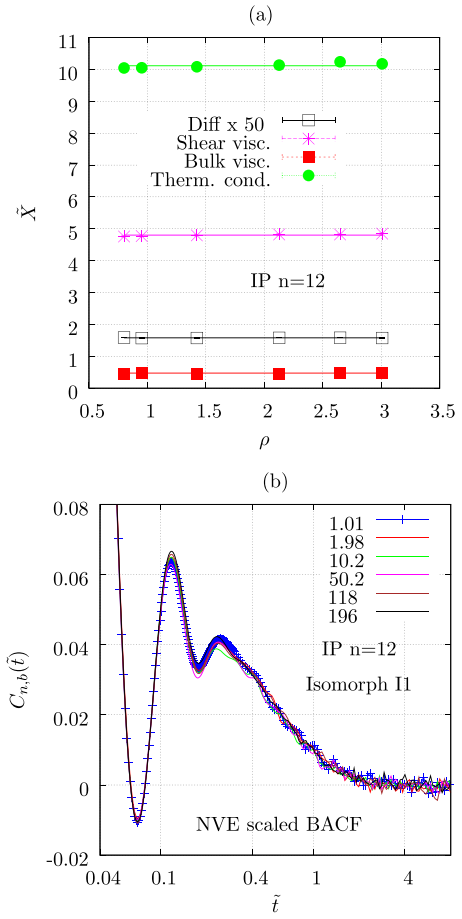

FIG. 8. Frame (a), the IU scaled four transport coefficients for an IPF (n = 12) or $\phi(r) = 4\epsilon(\sigma/r)^{12}$ fluid along the isomorph, $\rho = \rho_0(T/T_0)^{1/4}$, where $\rho_0 = 0.8$, $T_0 = 1.0$, which gives $\tilde{D} = 0.031\,59$, $\tilde{\eta}_s = 4.812\,75$, $\tilde{\eta}_b = 0.473\,29$, and $\tilde{\lambda} = 10.099$. This confirms that from the MD GK program, the bulk viscosity is invariant along an isomorph for the IPF system (as it should be). Frame (b) corresponds to Fig. 7(b), except that the BACF of the IP (n = 12) system is shown. The temperatures are given in the figure.

frequencies. The first is the second frequency moment, M_2, which can be calculated numerically to various orders of approximation from the first few values of the normalized time correlation function. Let $C_m = C_n(m\Delta t)$, where $m = 0, 1, 2, \ldots$, then[106,107]

$$\begin{aligned} C_n(t) &= 1 - M_2\frac{t^2}{2!} + O(t^4), \\ M_{2a} &= \frac{2}{\Delta t^2}(1 - C_1), \\ M_{2b} &= \frac{1}{\Delta t^2}\left(\frac{5}{2} - \frac{8}{3}C_1 + \frac{1}{6}C_2\right), \\ M_{2c} &= \frac{1}{90\Delta t^2}(245 - 270C_1 + 27C_2 - 2C_3), \end{aligned} \tag{21}$$

using polynomials of increasing order to represent the decay of the correlation function at short times. Note that $C_0 = 1$. The formal definition of M_2 is[107]

$$M_2 = \int_{-\infty}^{\infty}\omega^2 p(\omega)d\omega, \quad p(\omega) = \frac{1}{2\pi}\int_{-\infty}^{\infty} C_n(t)\exp(i\omega t)dt, \quad \text{where } \int_{-\infty}^{\infty} p(\omega)d\omega = 1. \tag{22}$$

The value of M_2 was computed for the four TC autocorrelation functions using Eq. (21), and an IU scaled equivalent frequency is then $\tilde{\Omega}_X = \sqrt{\tilde{M}_2}$ for each autocorrelation function derived from transport property X.

The second quantity with units of inverse time considered is the Einstein frequency, Ω_E,[108,109]

$$\begin{aligned} \Omega_E^2 &= \frac{4\pi\rho}{3m}\int_0^{\infty} dr\, r^2\left(\phi''_{LJ}(r) + \frac{2\phi'_{LJ}}{r}\right)g(r), \\ &\equiv \frac{2}{3Nm}\sum_{i<j}\left\langle\phi''_{LJ}(r_{ij}) + \frac{2\phi'_{LJ}(r_{ij})}{r_{ij}}\right\rangle \equiv \frac{\langle \boldsymbol{F}^2\rangle}{3k_BTm}, \end{aligned} \tag{23}$$

where m is the mass of the molecule and $\langle \boldsymbol{F}^2\rangle$ is the mean square force on a molecule at equilibrium. Ω_E is a dynamical quantity that can be expressed entirely in terms of static quantities.

Figure 9(a) presents the variation in Ω_X and Ω_E in LJ units along the isomorph I1 for the four transport coefficients. The increase in these frequencies is about an order of magnitude over the density range. For the VACF, the M_2 is formally the same as Ω_E^2, which is seen to be the case in the figure. Figure 9(b) shows the corresponding $\tilde{\Omega}_X$ and $\tilde{\Omega}_E$ in IU. The variation with density is much smaller, but they both decrease by about 5% toward the high density limit. For each transport coefficient, the M_2 value from the first three state points decreases monotonically until it reaches an asymptotic value at high temperature (density), for all apart from the BACF case that continues to decrease. Therefore, these high frequency limits for all TC show a small but significant departure from IU scaling for about the first three lower T (or ρ) state points at least.

D. Transport coefficients

Table III presents the transport coefficients computed here for the LJ liquid reference near triple point state point, $\rho = 0.8442$ and $T = 0.722$, which was first used by Levesque *et al.*[3] Values for the four transport coefficients at this state point taken from previous work are also presented in Table III. The two sets of data agree within their statistical uncertainties. Table III also lists the four transport coefficients in LJ units for the state points along the isomorph I1. The values of all TC along the isomorph are seen to increase by at least an order of magnitude on increasing density and temperature. This is noteworthy as along an isotherm, in contrast, it is usually found that the diffusion coefficient decreases with increasing density, while the shear viscosity increases,[110] certainly in the high density range.

Figure 10(a) shows D for the four isomorphs as a function of ρ, and Fig. 10(b) presents the corresponding $\tilde{D}$ values. Within the simulation statistics, $\tilde{D}$ is invariant along each isomorph for all ρ (except perhaps for a small dip for the $T = 0.8$ state point). Figure 11 shows the corresponding plots for the shear viscosity that is also seen to be invariant within statistics apart for T less than about 1.0.

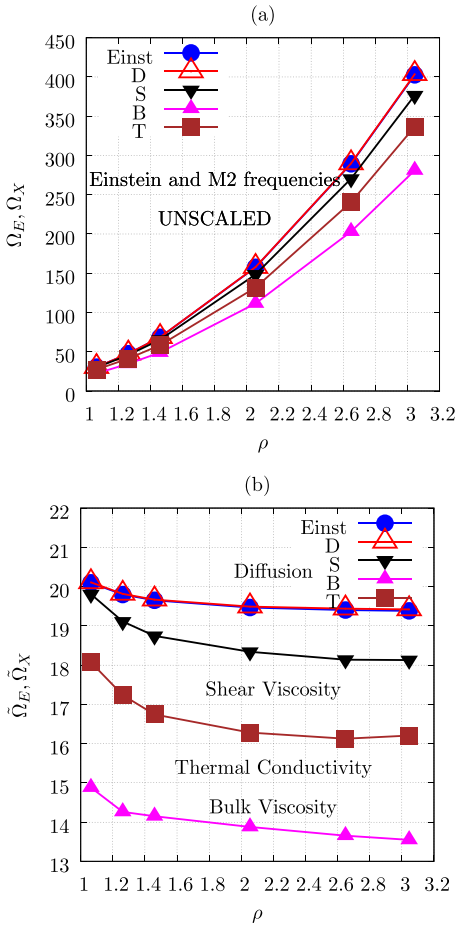

FIG. 9. The density dependence of the Einstein frequency,[108] Ω_E, defined in Eq. (23), and second moment, M_2, frequency, taken as the average of the three definitions in Eq. (21), and $\Omega_X = \sqrt{M_2}$. Key: $X \equiv D$, S, B, and T are for the self-diffusion, shear viscosity, bulk viscosity, and thermal conductivity time correlation functions, respectively. For the bulk viscosity, the frequency is scaled by 1/2. The MD simulations were for $N = 864$ particles along the isomorph I1. Frame (a) is in LJ units, while (b) is in IU.

Figure 12(a) demonstrates that the bulk viscosity increases monotonically with density along each isomorph and that these curves follow closely each other when expressed in LJ units, which indicates an insensitivity to temperature. In contrast, the IU scaled bulk viscosity given in Fig. 12(b) decreases noticeably with increasing density for the four isomorphs until it approaches an IP-like limit. The bulk viscosity cannot reasonably be claimed to be invariant along these isomorphs, certainly in the low density regime. The variable oscillatory region in the BACF shown in Fig. 7(b) is presumably the reason for this.

The corresponding thermal conductivity data are presented in Fig. 13. It is notable in Fig. 13(a) that λ in LJ units increases with density along each isomorph in the same temperature independent way within the simulation statistics. There is an approximate collapse of the data from the four isomorphs on the same curve. This is different behavior to the shear viscosity given in Fig. 11(a), which

TABLE III. The four transport coefficients in LJ units for a LJ reference state point and along the isomorph I1. The top row of data is taken from this work for the reference state point. The numbers in brackets are the estimated standard errors in the last digit. The D, η_s, and λ data were taken from NVT simulations, and the η_b values are from NVE simulations where the average temperatures during the simulations were 2.28, 4.70, 9.23, 40.7, 116.8, and 205.5 with increasing density. Key: Row "A" used NVT for D, η_s, and λ and NVE for η_b. The data are from the $N = 864$ sets of MD simulations.

T	ρ	D	η_s	η_b	λ
0.722[A]	0.8442	0.032 1(2) 0.0327(2)[113]	3.26(6) 3.29(3)[6] 3.29(6)[7]	1.20(3) 1.22(3)[42] 1.16(1)[11]	6.95(5) 6.99(3)[13]
2.2000	1.0635	0.046 18(8)	7.32(3)	1.18(2)	15.09(7)
4.9179	1.2617	0.065 7(2)	12.2(1)	1.67(1)	25.8(1)
9.4388	1.4599	0.086 9(2)	18.72(8)	2.27(2)	39.5(2)
40.593	2.0545	0.161 1(4)	48.0(2)	5.23(6)	103.7(5)
116.22	2.6491	0.251 7(6)	97.2(5)	9.8(1)	209(1)
205.58	3.0455	0.318 6(8)	141.3(7)	14.3(2)	305(2)

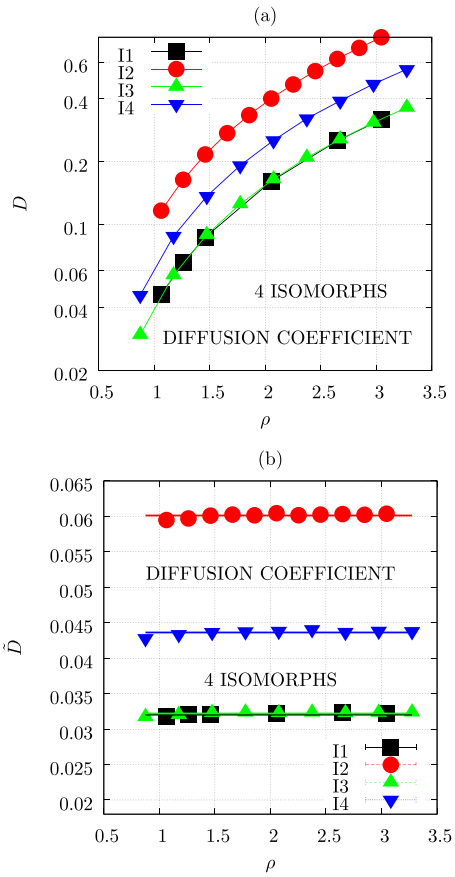

FIG. 10. Frame (a), the unscaled ("LJ") self-diffusion coefficient, D, as a function of density for the four isomorphs (note the lin-log scale). Frame (b) shows the same self-diffusion coefficients as in frame (a) but IU scaled. Note the excellent invariance in IU units in frame (b). The $\langle \tilde{D} \rangle$ values are 0.032 04, 0.060 12, 0.032 20, and 0.043 63, for the 4 isomorphs I1 to I4, respectively.

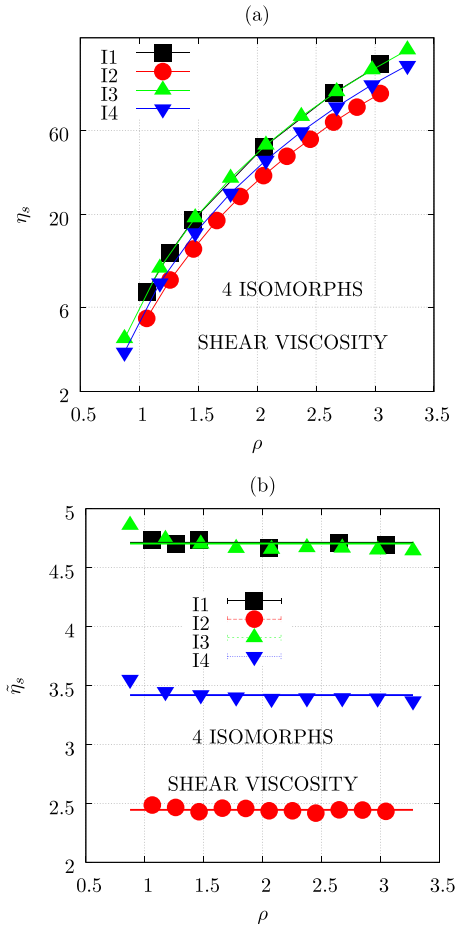

FIG. 11. As for Fig. 10, except the shear viscosity isomorph values are presented. In frame (a), η_s is given in LJ ("unscaled") units, and in frame (b), $\tilde{\eta}_s$ is shown. Note the isomorphic collapse at not too low temperatures in frame (b). The $\langle\tilde{\eta}_s\rangle$ for the isomorphs I1 to I4 are 4.71, 2.45, 4.704, and 3.42, respectively.

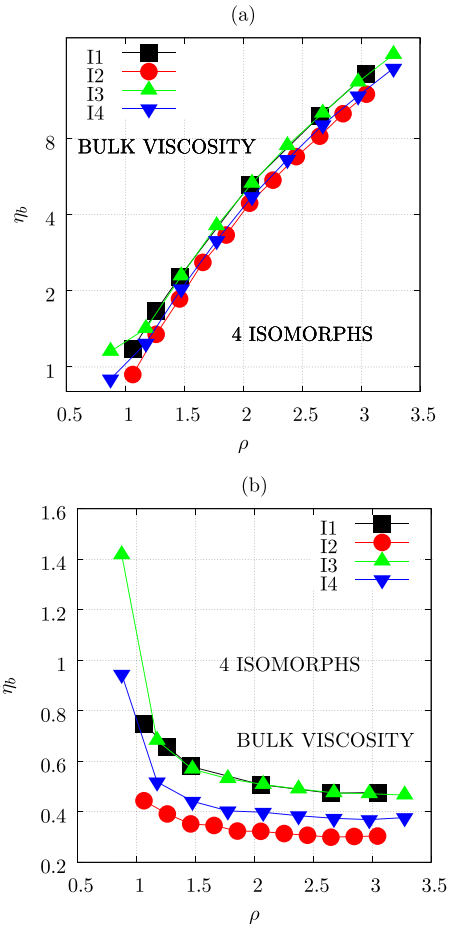

FIG. 12. The unscaled bulk viscosity, η_b, of the four isomorphs in frame (a) (note the lin-log scale) and IU-scaled, $\tilde{\eta}_b$, in frame (b). Note the failure of isomorphic collapse in frame (b).

shows that the four isomorphs are approximately parallel but not coincident. Figure 13(b) reveals that the $\tilde{\lambda}$ are within the simulation statistical uncertainty invariant along the isomorphs to a very good approximation (again apart from showing some small decrease for temperatures below about 1.0). The scaled $\tilde{\lambda}(\rho)$ are more noisy than the $\tilde{\eta}_s(\rho)$, possibly because the heat flux expression in Eq. (11) involves the difference in velocity for the two molecules in the pair summation.

Figures 14 and 15 present the IU scaled transport coefficients $\tilde{D}$, $\tilde{\eta}_s$, $\tilde{\eta}_b$, and $\tilde{\lambda}$ normalized by their high temperature limiting values. The highest three temperature (density) state points were used to obtain these limits, which are denoted by $\langle\tilde{D}\rangle$, $\langle\tilde{\eta}_s\rangle$, and $\langle\tilde{\lambda}\rangle$. The highest temperature state point was used to assign this limit for $\tilde{\eta}_b$ because of its monotonic decay with density (no limiting plateau at high density is evident). These averages are therefore obtained over a limited number of state points for which the $\tilde{X}$ are more likely to be invariant. The quantity, $\tilde{X}_n = \tilde{X}/\langle\tilde{X}\rangle$, is plotted with density for the four TC in the figures. The relaxation or correlation times, τ_c, and moduli ("M"), defined in Eqs. (2), (3), (10), and (13), respectively, are also presented in the figures and normalized in the same way. Data for N = 864, 2048, and 4000 are shown in each figure.

Figure 14(a) gives the normalized IU scaled diffusion coefficients, $\tilde{D}_n(\rho)$, for isomorph I1, which shows that for the three system sizes they are all indistinguishable within the simulation statistics (note the fine scale of the abscissa). The maximum deviation from invariancy is about 1%. Figure 14(b) presents the shear viscosity, instantaneous shear modulus, G_∞, and shear relaxation time, $\tau_{s,n}$, from Eq. (3), all IU scaled and normalized. The $\tilde{G}_{\infty,n}$ decrease to the limiting value of unity with increasing ρ, while $\tilde{\tau}_s$ increases to the same limit. As these trends are in the opposite direction, their effects on $\tilde{\eta}_{s,n}$ largely cancel, leaving an invariant $\tilde{\eta}_{s,n}$ within about 2% across the density range. This is despite the fact that as was proved in Sec. II E, the LJ $\tilde{G}_\infty$ is not invariant along an isomorph (although we only find about 10% deviations). The earliest approximate statistical mechanical theories of the shear viscosity are cast in

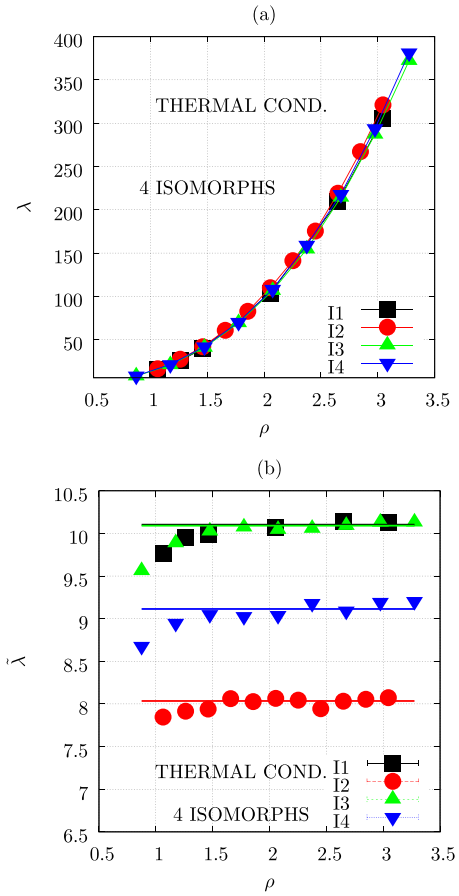

FIG. 13. The thermal conductivity in LJ units of the four isomorphs in frame (a) (note the lin-log scale) and IU-scaled in frame (b). There is very good isomorphic collapse at not too low densities in frame (b). The $\langle\tilde{\lambda}\rangle$ are 10.10, 8.03, 10.09, and 9.11 for the four isomorphs, respectively.

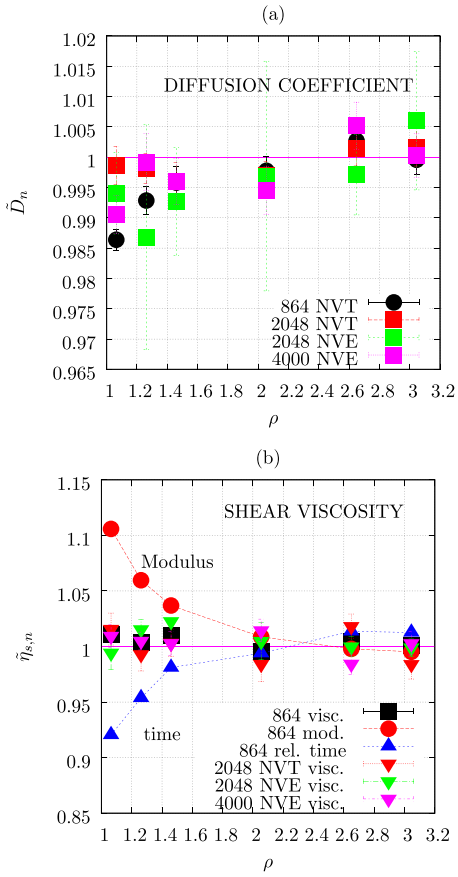

FIG. 14. Frame (a), the density dependence of the normalized self-diffusion coefficient from Eq. (2) for the I1 isomorph. The ratio, $\tilde{D}_n = \tilde{D}/\langle\tilde{D}\rangle$, is plotted against density, where for $N = 864$, $\langle\tilde{D}\rangle = 0.032\,19(4)$, and $\langle\tilde{D}\rangle$ is the average of the highest three densities and for 2048 $\langle\tilde{D}\rangle = 0.033\,01(5)$. Frame (b) presents the shear viscosity, η_s, G_∞, and τ_s data from Eq. (3) for the IP1 isomorph. Key: For the viscosity, modulus, and relaxation time, the $\langle\tilde{X}\rangle$ for N = 864 are 4.69(1), 33.3(1), and 0.140(1) for the viscosity, modulus, and relaxation time, respectively, and for 2048 particles, these quantities are 4.66(6), 33.3(1), and 0.141(2).

terms of integrals of the radial distribution function,[20–23] from which it would follow that the viscosity should be isomorph invariant in macroscopic reduced units as the RDFs are invariant, as is demonstrated in Fig. 14(b). The modulus and viscosity are formally and independently defined analytically, and they therefore determine the observed behavior in the relaxation time.

Figure 15(a) presents the bulk viscosity data as $\tilde{\eta}_{b,n}(\rho)$ and the associated modulus and relaxation time. In this case, both modulus and relaxation time decrease with increasing ρ, which is consistent with the conclusion derived from Fig. 12 that the IU scaled bulk viscosity is not invariant along an isomorph. The increase in viscosity is mainly accounted for by the modulus, though, leaving the relaxation time more invariant, as for the shear.

Figure 15(b) shows the corresponding thermal conductivity data and reveals that $\tilde{\lambda}_n$, and the modulus and relaxation time quantities show the same trends as the shear viscosity given in Fig. 14(b) (i.e., the deviations mainly cancelling each other out). This explains why $\tilde{\lambda}$ is to a very good approximation isomorph invariant.

The fundamental question remains, why does the bulk viscosity show qualitatively different trends to the two other collective property transport coefficients? The D, η_s, and λ involve quantities in their GK correlation function definition whose time average at equilibrium is zero and are therefore not formally linked to the thermodynamic state of the system (although these quantities are state point dependent). The definition of the bulk viscosity in contrast is inextricably dependent on the thermodynamic state, whose basic quantities, such as total energy and pressure are not isomorph invariant, as proved in Sec. II E. Table IV gives the moduli relevant to the transport coefficients computed for the LJ reference state, $\rho = 0.8442$ and $T = 0.722$, as well as the moduli for the I1 state points.

For a step in bulk "strain," $\delta\gamma = -[\delta\rho/\rho]$ resulting from a step in density, $\delta\rho$, applied to an NVE simulation, the system moves immediately to a new value of the total energy, $E + \delta E$ at time $t = 0^+$. As $t \to \infty$, a new equilibrium pressure and temperature are

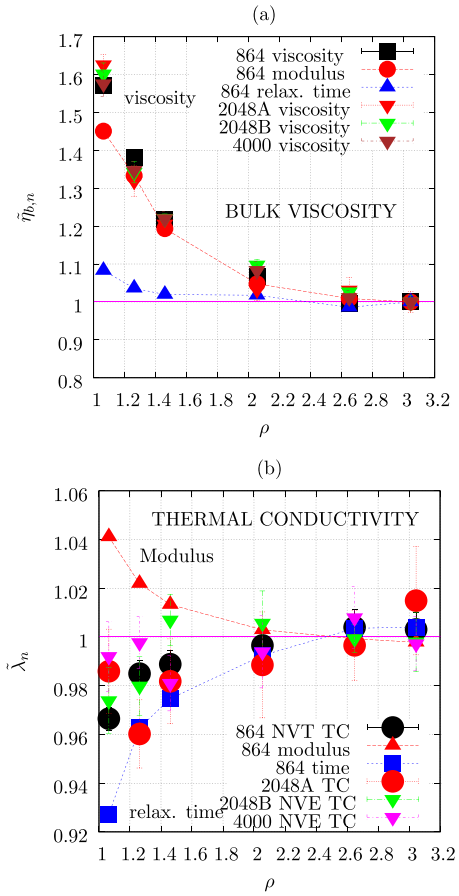

FIG. 15. Frame (a), the bulk viscosity, $K_\infty - K_0$, and τ_b data from Eq. (10) are plotted. Key: For the bulk viscosity, modulus, and relaxation time, the $\langle \tilde{X} \rangle$ for N = 864 are 0.474, 8.3748, 0.056 634, and for N = 2048 for the viscosity, 0.462. Frame (b), the thermal conductivity and related quantities given in Eq. (13) are plotted against density. Key: For the thermal conductivity, modulus, and relaxation time, the $\langle \tilde{X} \rangle$ for N = 864 are 10.10(3), 103.7(2), and 0.0975(4) for λ, the modulus, and relaxation time, respectively. For N = 2048, these quantities are 10.16(8), 104.0(2), and 0.0977(8).

eventually reached at a rate which is determined by the time correlation function of the deviatoric pressure. The time dependent pressure, $P(t)$, is obtained directly from the time dependent bulk modulus, $K(t)$,[111] via

$$K(t) = K_0(0^-) + \frac{V}{k_B T}\langle \delta P(0)\delta P(t)\rangle,$$
$$P(t) = P(0^-) + \delta\gamma K_0 + \delta\gamma \frac{V}{k_B T}\langle \delta P(0)\delta P(t)\rangle. \quad (24)$$

As $(K_\infty - K_0) = (V/k_B T)\,\langle \delta P(0)\delta P(0)\rangle$, then

$$P(0^+) = P(0^-) + \delta\gamma K_\infty,$$
$$P(t \to \infty) = P(0^-) + \delta\gamma K_0, \quad (25)$$

(note that the correlation function tends to zero at long times). Equation (25) contains useful generic relationships but does not indicate how the correlation function depends on the ensemble employed in an MD simulation. The bulk viscosity is given by the time integral of the time correlation function as specified in Eq. (10). $P(t)$ depends on the time dependent modulus, $K(t)$, which makes the correlation function (and hence η_b) a nontrivial function of the evolution of the static property variables of the new state point to their equilibrium values. The situation is more straightforward for the shear viscosity because the long time or zero frequency limit modulus is zero (except for a solid[112]). We already know that the pressure and moduli are not invariant along an isomorph for the LJ fluids, so the relative failure of η_b to be constant along an isomorph follows from this more complex dependence of the deviatoric pressure on the evolving system's thermodynamic state.

TABLE IV. As for Table III, except that the moduli associated with η_s, η_b, and λ are presented. Key: The simulations employed 864 particles. The G_∞, K_∞, and M_∞ data were taken from *NVT* simulation, and the $K_\infty - K_0$ values are from *NVE* simulations where the average temperatures during the simulations were 2.28, 4.70, 9.23, 40.7, 116.8, and 205.5 with increasing density.

T	ρ	G_∞	K_∞	$K_\infty - K_0$	M_∞
0.722	0.8442	23.98(5) 23.9[3]	40.06(2)	15.20(6)	66.4(3)
2.2000	1.0635	86.14(3)	368.4	29.3(2)	252.7
4.9179	1.2617	218.9(1)	1 021	65.7(3)	657.9
9.4388	1.4599	475.7(2)	2 318	133.7(6)	1 449(1)
40.593	2.0545	2 801(1)	14 423	728(6)	8 678(6)
116.22	2.6491	10 229(4)	53 769	2596(10)	31 918(12)
205.58	3.0455	2 075(1)	109 720	5202(23)	64 815(38)

IV. CONCLUSIONS

Isomorphs are lines of constant excess entropy that in the dense fluid regime approximately follow the freezing line. The isomorphs studied here occupy a considerable part of the fluid phase diagram, covering a temperature range of two orders of magnitude and a factor of 3–4 in density, which are "geological" scale changes. Only the inverse power (IP) potential fluid is exactly isomorphic (i.e., in exhibiting property invariance when expressed in Rosenfeld's macroscopic units) along an isomorph. Nevertheless, the Lennard-Jones system by virtue of the specially determined density-temperature dependence of the isomorph shows invariance of most of its properties to a degree that is almost as good as the IP case, even for temperatures as low as ~1.0 in LJ reduced units, which is close to the triple point. It is shown here that along the isomorphs of the Lennard-Jones system, structural, static, and dynamical properties are to varying degrees nearly invariant. In contrast to previous studies, the time correlation function-based Green-Kubo formulas are used to analyze the isomorphic scaling of the Lennard-Jones transport coefficients.

The purely structural properties show the best degree of invariance, closely followed by the transport coefficients (apart from the bulk viscosity) even though the elastic moduli are not invariant. This

is proved for the first time for thermal conductivity. The elastic moduli are simple functions of the number density and two "structural" parameters that are invariant along an isomorph. The bulk viscosity is the exception as it is (unlike the other transport coefficients) defined in terms of a perturbation that changes the thermodynamic state of the system. The manifestation of this difference takes the form of oscillations in the pressure autocorrelation function at intermediate times that do not collapse when plotted in macroscopic units (unlike the behavior of a comparable inverse power potential system).

It is possible that for experimental systems consisting of particles that are much softer than described by the Lennard-Jones potential, the scaling of the bulk viscosity would be better, as the stress relaxation functions for these systems would be less likely to decay in an oscillatory manner. It is the oscillatory behavior of the pressure relaxation function that appears to be the source of the departures from isomorphic invariance for the bulk viscosity along an isomorph for the Lennard-Jones system. From an experimental perspective, traction fluids are more likely to behave as LJ fluids,[114–116] while squalene and other alkanes in general should be better represented by soft (low exponent) IP fluids. Also, molecules that inhibit liquid crystallization[116] might control the bulk viscosity better for specific lubrication applications.

SUPPLEMENTARY MATERIAL

The numerical data for calculated properties of the four isomorphs are presented in a tabular form in the supplementary material.

ACKNOWLEDGMENTS

D.D. and D.M.H. would like to acknowledge the support received from the EPSRC under the Established Career Fellowship Grant No. EP/N025954/1. All data can be made available by emailing the authors of the paper or to tribology@imperial.ac.uk. This work was supported by the VILLUM Foundation's *Matter* Grant (No. 16515) and a research Grant (No. 00023189) from VILLUM FONDEN. We thank a reviewer for helpful suggestions to improve the manuscript.

REFERENCES

[1] J.-P. Hansen and I. R. McDonald, *Theory of Simple Liquids*, 4th ed. (Academic Press, Amsterdam, 2013).
[2] D. Levesque and L. Verlet, Phys. Rev. A **2**, 2514 (1970).
[3] D. Levesque, L. Verlet, and J. Kürkijarvi, Phys. Rev. A **7**, 1690 (1973).
[4] K. Meier, A. Laesecke, and S. Kabelac, J. Chem. Phys. **121**, 9526 (2004).
[5] V. G. Baidakov, S. P. Protsenko, and Z. R. Kozlova, Fluid Phase Equilib. **305**, 106 (2011).
[6] K. Meier, A. Laesecke, and S. Kabelac, J. Chem. Phys. **121**, 3671 (2004).
[7] S. Viscardy, J. Servantie, and P. Gaspard, J. Chem. Phys. **126**, 184512 (2007).
[8] D. M. Heyes, Can. J. Phys. **64**, 773 (1986).
[9] D. M. Heyes, J. Chem. Soc., Faraday Trans. 2 **80**, 1363 (1984).
[10] F. Jaeger, O. K. Matar, and E. A. Müller, J. Chem. Phys. **148**, 174504 (2018).
[11] K. Meier, A. Laesecke, and S. Kabelac, J. Chem. Phys. **122**, 014513 (2005).
[12] M. Bugel and G. Galliero, Chem. Phys. **352**, 249 (2008).
[13] S. Viscardy, J. Servantie, and P. Gaspard, J. Chem. Phys. **126**, 184513 (2007).
[14] M. P. Lautenschlaeger, M. Horsch, and H. Hass, Mol. Phys. **117**, 189 (2018).
[15] G. Galliero and C. Boned, Phys. Rev. E **80**, 061202 (2009).
[16] B. Y. Baharudin, D. A. Jackson, and P. E. Schoen, Phys. Lett. A **51**, 409 (1975).
[17] T. A. Litovitz and C. M. Davis, in *Physical Acoustics*, edited by W. P. Mason (Academic Press, New York, 1964), Vol. 2, Chap. 5.
[18] A. R. Eastwood, J. Chem. Soc., Faraday Trans. 2 **76**, 704 (1980).
[19] H. Spikes and Z. Jie, Tribol. Lett. **56**, 1 (2014).
[20] J. G. Kirkwood, F. P. Buff, and M. S. Green, J. Chem. Phys. **17**, 988 (1949).
[21] B. A. Lowry, S. A. Rice, and P. Gray, J. Chem. Phys. **40**, 3673 (1964).
[22] K. Rah and B. C. Eu, J. Chem. Phys. **114**, 10436 (2001).
[23] R. W. Zwanzig, J. G. Kirkwood, I. Oppenheim, and B. J. Alder, J. Chem. Phys. **22**, 783 (1954).
[24] P. L. Palla, C. Pierleoni, and G. Ciccotti, Phys. Rev. E **78**, 021204 (2008).
[25] K. Tankeshwar, J. Phys.: Condens. Matter **6**, 9295 (1994).
[26] K. Tankeshwar, K. N. Pathak, and S. Ranganathan, J. Phys.: Condens. Matter **8**, 10847 (1996).
[27] D. Bertolini and A. Tani, J. Chem. Phys. **115**, 6285 (2001).
[28] K. Rah and B. C. Eu, Phys. Rev. Lett. **83**, 4566 (1999).
[29] A. S. Dukhin and P. J. Goetz, J. Chem. Phys. **130**, 124519 (2009).
[30] A. C. Brańka and D. M. Heyes, Phys. Rev. E **69**, 021202 (2004).
[31] J. W. Dufty, Granular Matter **14**, 271 (2012).
[32] A. Santos, J. M. Montanero, J. W. Dufty, and J. J. Brey, Phys. Rev. E **57**, 1644 (1998).
[33] P. Gray and S. A. Rice, J. Chem. Phys. **41**, 3689 (1964).
[34] B. J. Alder, D. M. Gass, and T. E. Wainwright, J. Chem. Phys. **53**, 3813 (1970).
[35] W. G. Hoover, D. J. Evans, R. B. Hickmann, A. J. C. Ladd, W. T. Ashurst, and B. Moran, Phys. Rev. A **22**, 1690 (1980).
[36] D. M. Heyes, J. Chem. Soc., Faraday Trans. 2 **79**, 1741 (1983).
[37] S. K. Das, J. Horbach, and K. Binder, Phase Transitions **77**, 823 (2004).
[38] C. Hoheisel, R. Vogelsang, and M. Schoen, J. Chem. Phys. **87**, 7195 (1987).
[39] V. G. Baidakov and S. P. Protsenko, J. Chem. Phys. **141**, 114503 (2014).
[40] H. Okumura and F. Yonezawa, J. Chem. Phys. **116**, 7400–7410 (2002).
[41] H. Okumura and F. Yonezawa, Phys. Rev. E **67**, 021205 (2003).
[42] J. J. Erpenbeck, Phys. Rev. A **38**, 6255 (1988).
[43] G.-J. Guo and Y.-G. Zhang, Mol. Phys. **99**, 283 (2001).
[44] R. Castillo and S. Castañeda, Int. J. Thermophys. **9**, 383 (1988).
[45] J. F. Ely and H. J. M. Hanley, Ind. Eng. Chem. Fundam. **22**, 90 (1983).
[46] A. J. H. McGaughey and M. Kaviany, Int. J. Heat Mass Transfer **47**, 1783 (2004).
[47] H. M. Roder, C. A. Nieto de Castro, and U. V. Mardolcar, Int. J. Thermophys. **8**, 521 (1987).
[48] M. J. Assael, J. H. Dymond, P. Papadaki, and P. M. Patterson, Fluid Phase Equilib. **75**, 245 (1992).
[49] J. C. Dyre, Phys. Rev. E **88**, 042139 (2013).
[50] E. A. Guggenheim, J. Chem. Phys. **13**, 253 (1945).
[51] K. D. Hammonds and D. M. Heyes, J. Chem. Soc., Faraday Trans. 2 **84**, 705 (1988).
[52] R. Casalini and C. M. Roland, Phys. Rev. E **69**, 062501 (2004).
[53] R. Casalini, U. Mohanty, and C. M. Roland, J. Chem. Phys. **125**, 014505 (2006).
[54] T. S. Ingebrigtsen, T. B. Schrøder, and J. C. Dyre, Phys. Rev. X **2**, 011011 (2012).
[55] J. C. Dyre, J. Phys.: Condens. Matter **28**, 323001 (2016).
[56] I. H. Bell, R. Messerley, M. Thol, L. Costigliola, and J. C. Dyre, J. Phys. Chem. B **123**, 6345 (2019).
[57] L. Costigliola, D. M. Heyes, T. B. Schrøder, and J. C. Dyre, J. Chem. Phys. **150**, 021101 (2019).
[58] J. J. Erpenbeck, Phys. Rev. E **51**, 4296 (1995).
[59] J. C. Maxwell, Philos. Trans. R. Soc. London **157**, 49 (1867).
[60] R. Zwanzig and R. D. Mountain, J. Chem. Phys. **43**, 4464 (1965).
[61] D. M. Heyes, J. Chem. Soc., Faraday Trans. 2 **85**, 239 (1989).
[62] T. S. Ingebrigtsen, L. Bøhling, T. B. Schrøder, and J. C. Dyre, J. Chem. Phys. **136**, 061102 (2012).
[63] E. Helfand, Phys. Rev. **119**, 1 (1960).
[64] J. A. McLennan, Prog. Theor. Phys. **30**, 408 (1963).
[65] S. Toxvaerd, J. Chem. Phys. **137**, 214102 (2012).

[66]S. Toxvaerd, J. Chem. Phys. **139**, 224106 (2013).
[67]D. M. Heyes and J. G. Powles, Mol. Phys. **99**, 1077 (2001).
[68]A. E. Nasrabad, N. M. Oghaz, and B. Haghighi, J. Chem. Phys. **129**, 024507 (2008).
[69]Y. Rosenfeld, J. Chem. Phys. **63**, 2769 (1975).
[70]Y. Rosenfeld, Mol. Phys. **32**, 963 (1976).
[71]Y. Rosenfeld, Phys. Rev. E **62**, 7524 (2000).
[72]T. B. Schrøder, N. Gnan, U. R. Pedersen, N. P. Bailey, and J. C. Dyre, J. Chem. Phys. **134**, 164505 (2011).
[73]L. Bøhling, A. A. Veldhorst, T. S. Ingebrigtsen, N. P. Bailey, J. S. Hansen, S. Toxvaerd, T. B. Schrøder, and J. C. Dyre, J. Phys.: Condens. Matter **25**, 032101 (2013).
[74]G. Rickayzen and D. M. Heyes, J. Phys.: Condens. Matter **19**, 416101 (2007).
[75]A. Baranyai and D. J. Evans, Phys. Rev. A **40**, 3817 (1989).
[76]Y. Rosenfeld, Phys. Rev. A **15**, 2545 (1977).
[77]Y. Rosenfeld, J. Phys.: Condens. Matter **11**, 5415 (1999).
[78]J. H. Dymond, Int. J. Thermophys. **18**, 303 (1997).
[79]D. M. Heyes, *The Liquid State: Applications of Molecular Simulations* (Wiley, Chichester, 1998).
[80]W. G. Hoover, Phys. Rev. A **31**, 1695 (1985).
[81]M. P. Allen and D. J. Tildesley, *Computer Simulation of Liquids* (Oxford UP, Oxford, 2017).
[82]L. Bøhling, T. S. Ingebrigtsen, A. Grzybowski, M. Paluch, J. C. Dyre, and T. B. Schrøder, New J. Phys. **14**, 113035 (2012).
[83]L. Costigliola, T. B. Schrøder, and J. C. Dyre, Phys. Chem. Chem. Phys. **18**, 14678 (2016).
[84]L. Costigliola, "Isomorph theory and extensions," Ph.D. dissertation (Roskilde University, Denmark, 2016).
[85]U. R. Pedersen, L. Costigliola, N. P. Bailey, T. B. Schrøder, and J. C. Dyre, Nat. Commun. **7**, 12386 (2016).
[86]A. Lofti, J. Vrabec, and J. Fischer, Mol. Phys. **76**, 1319 (1992).
[87]D. M. Heyes, Comput. Methods Sci. Technol. **21**, 169 (2015).
[88]S. Pieprzyk, A. C. Brańka, Sz. Maćkowiak, and D. M. Heyes, J. Chem. Phys. **148**, 114505 (2018).
[89]D. M. Heyes and A. C. Brańka, J. Chem. Phys. **143**, 234504 (2015).
[90]U. R. Pedersen, J. Chem. Phys. **139**, 104102 (2013).
[91]A. J. Schultz and D. A. Kofke, J. Chem. Phys. **149**, 204508 (2018).
[92]S. A. Khrapak, M. Chaudhuri, and G. E. Morfill, Phys. Rev. E **82**, 052101 (2010).
[93]S. A. Khrapak and G. E. Morfill, J. Chem. Phys. **134**, 094108 (2011).
[94]L. Separdar, N. P. Bailey, T. B. Schrøder, S. Davatolhagh, and J. Dyre, J. Chem. Phys. **138**, 154505 (2013).
[95]N. P. Bailey, U. R. Pedersen, N. Gnan, T. B. Schrøder, and J. C. Dyre, J. Chem. Phys. **129**, 184508 (2008).
[96]U. R. Pedersen, N. P. Bailey, T. B. Schrøder, and J. C. Dyre, Phys. Rev. Lett. **100**, 015701 (2008).
[97]S. Toxvaerd and J. C. Dyre, J. Chem. Phys. **135**, 134501 (2011).
[98]P. Krüger, S. K. Schnell, D. Bedeaux, S. Kjelstrup, T. J. H. Vlugt, and J.-M. Simon, J. Phys. Chem. **4**, 235 (2013).
[99]U. R. Pedersen, T. B. Schrøder, and J. C. Dyre, Phys. Rev. Lett. **120**, 165501 (2018).
[100]F. H. Stillinger, J. Chem. Phys. **38**, 1486 (1963).
[101]D. M. Heyes, M. J. Cass, and A. C. Brańka, Mol. Phys. **104**, 3137 (2006).
[102]N. Gnan, T. B. Schrøder, U. R. Pedersen, N. P. Bailey, and J. C. Dyre, J. Chem. Phys. **131**, 234504 (2009).
[103]T. B. Schrøder and J. C. Dyre, J. Chem. Phys. **141**, 204502 (2014).
[104]A. K. Bacher, T. B. Schrøder, and J. C. Dyre, J. Chem. Phys. **149**, 114501 (2018).
[105]C. Hoheisel, J. Chem. Phys. **86**, 2328 (1987).
[106]D. M. Heyes and J. G. Powles, Mol. Phys. **71**, 781 (1990).
[107]D. M. Heyes, J. G. Powles, and J. C. Gil Montero, Mol. Phys. **78**, 229 (1993).
[108]U. Balucani and M. Zoppi, *Dynamics of the Liquid State* (Clarendon Press, Oxford, 1994), p. 290.
[109]T. Young and H. C. Andersen, J. Phys. Chem. B **109**, 2985 (2005).
[110]D. M. Heyes, Phys. Rev. E **37**, 5677 (1988).
[111]J. K. Nielsen, Phys. Rev. E **60**, 471 (1990).
[112]S. R. Williams and D. J. Evans, J. Chem. Phys. **131**, 024115 (2009).
[113]K. Takahashi, K. Yasuoka, and T. Narumi, J. Chem. Phys. **127**, 114511 (2007).
[114]J. P. Ewen, C. Gattinoni, J. Zhang, D. M. Heyes, H. A. Spikes, and D. Dini, Phys. Chem. Chem. Phys. **19**, 17883 (2017).
[115]D. M. Heyes, E. R. Smith, D. Dini, H. A. Spikes, and T. A. Zaki, J. Chem. Phys. **136**, 134705 (2012).
[116]C. Gattinoni, D. M. Heyes, C. D. Lorenz, and D. Dini, Phys. Rev. E **88**, 052406 (2013).